Research Article | Vol. 27, No. 25 / 9 December 2019 / Optics Express 36340
Optics EXPRESS

New insights into the thermal behavior and management of thermophotovoltaic systems

ETIENNE BLANDRE,[1,*] RODOLPHE VAILLON,[2] AND JÉRÉMIE DRÉVILLON[1]

[1] Institut Pprime, CNRS, Université de Poitiers, ISAE-ENSMA,F-86962 Futuroscope Chasseneuil, France
[2] IES, Univ Montpellier, CNRS, Montpellier, France
[*] etienne.blandre@univ-poitiers.fr

Abstract: The thermal behavior of a thermophotovoltaic system composed of a metallo-dielectric spectrally selective radiator at high temperature and a GaSb photovoltaic cell in the far field is investigated. Using a coupled radiative, electrical and thermal model, we highlight that, without a large conductive-convective heat transfer coefficient applied to the cell, the rise in temperature of the photovoltaic cell induces dramatic efficiency losses. We then investigate solutions to mitigate thermal effects, such as radiative cooling or the decrease of the emissivity or the temperature of the radiator. Without extending the radiating area beyond that of the cell, gains by radiative cooling are marginal. However, for a given radiator temperature, decreasing its emissivity is beneficial to conversion efficiency and, in cases of limited conductive-convective cooling capacities, even leads to larger electrical power outputs. More importantly, for a realistic radiator structure made of tungsten and hafnium oxide, larger conversion efficiencies are reached with smaller radiator temperatures because thermal losses and thus needs for cooling are less.

1. Introduction

Thermophotovoltaics (TPV) is a promising technology for converting heat into electricity using a high-temperature radiator emitting thermal radiation toward a low-bandgap photovoltaic (PV) cell [1]. Several experimental studies assessed the validity of the concept of thermophotovoltaic energy converters, with increasing efficiencies [2–6], recently reaching promising efficiency around 29% [7]. During the past years, many studies focused mainly on tailoring the spectral emission of the radiator [8–18] or the PV cell [19] such that the energy of the emitted photons are selected with respect to the bandgap of the PV cell, using various geometries and materials. Later, an emphasis was put on using materials withstanding high temperatures, like tungsten or molybdenum, such that the radiator is thermally stable and keeps its spectral selectivity at high-temperature. Thermal stability of some selective radiators was experimentally assessed [20–26]. If a lot of attention was paid to the spectral heat flux between the thermal radiator and the cell, the electrical and thermal behaviors of the PV cell were, however, often neglected. In this paper, we highlight the issue of the increase in temperature of the cell, and its impact on the performances of the TPV system.

Mostly because of thermalization of high energy photons, absorption of photons with sub-bandgap energy and recombination of electron-hole pairs inside the PV device, heat sources are generated in PV cells under illumination. Without a sufficient cooling power, this increase in temperature can lead to dramatic losses in efficiency, as the performances of the cell decreases with the cell temperature. These so-called thermal losses are a common issue in standard solar PV [27], where the incident solar radiative power is of the order of 1 kW.m^{-2}. In TPV, radiative heat fluxes involved can be orders of magnitude larger. This means thermal losses are likely to be extremely large, with a dramatic impact on the system efficiency. Studies involving thermal impacts in TPV devices were primarily focused on the near-field configuration [28,29], a particular case where radiative heat fluxes between the radiator and the cell are greatly enhanced

#377270 https://doi.org/10.1364/OE.27.036340
Journal © 2019 Received 10 Sep 2019; revised 14 Nov 2019; accepted 15 Nov 2019; published 27 Nov 2019

Optics EXPRESS

due to the contribution of evanescent waves. In tis case, it was highlighted that maintaining the cell at ambient temperature requires a conductive-convective heat transfer coefficient of 10^4 W.m^{-2}.K^{-1}, which is a value far beyond what can be obtained with passive cooling systems. In another work [30], it was shown that the optimal emission spectrum of a far-field TPV radiator is dramatically modified if thermal effects are accounted for, since high-energy photons generate heat via thermalization, and can decrease the performances of the system. In summary, it is important to account for thermal effects when designing TPV systems.

Cooling the PV cell is a solution for mitigating the thermal losses, but since active cooling systems use electrical energy, the overall efficiency system would be decreased. Therefore, the aims of this paper are: (i) to estimate the impact of thermal effects in a realistic TPV system consisting of a 1D multilayer spectrally selective radiator made of W and HfO_2 and a p-on-n GaSb junction. Radiative heat transfer from the emitter to the cell, transport of electrical charges and recombinations inside the p-n junction and variations of the cell temperature are accounted for in our simulation model; (ii) to evaluate the needs in terms of cooling to reach acceptable conversion performances, by considering conductive-convective heat transfer and passive radiative cooling; (iii) to seek for solutions to mitigate heat sources and decrease the cell temperature, such as decreasing the thermal emission of the radiator, and analyze the impact of doing so on the system performances.

2. Modelling of the TPV system

Lateral dimensions are assumed to be much larger than the thickness of the system, such that a 1D-Cartesian modelling is used. Radiative heat transfer between the radiator and the PV cell is computed within the frame of fluctuational electrodynamics [31,32] in conjunction with the S-matrix approach [33]. The calculated radiative power absorbed by the PV cell is then used to compute the local generation rate of electron-hole pairs G within control volumes formed by the spatially discretization of the PV device [28–30,34]

$$G(z) = \frac{\kappa^j_{\mathrm{IB}}}{\hbar\omega}\left(\frac{q^j_{\mathrm{abs}}}{\Delta z}\right), \tag{1}$$

z being the variable of space inside the p-n junction, κ the absorption coefficient of GaSb, Δz the size of a control volume, and q^j_{abs} the radiative power absorbed by a control volume. The subscript IB denotes the interband absorption process.

The local generation rate is required to solve the minority carrier diffusion equations in the quasi-neutral regions of the p-n junction.

$$D_{e,\,h}\frac{d^2\Delta n,\ p(z)}{dz^2} - \frac{\Delta n,\ p}{\tau_{e,\,h}} + G\,(z) = 0, \tag{2}$$

where the subscripts e and h stand for electrons and holes respectively, $\Delta n, p$ is the excess density of minority carriers (n for electrons and p for holes), D is the diffusion coefficient of minority carriers, and τ is the lifetime of minority carriers accounting for radiative, Auger and Shockley-Read-Hall recombination processes. The width of the depletion W_{dp} is calculated as

$$W_{\mathrm{dp}} = \left[\frac{2\varepsilon_s}{e}V_0\left(\frac{1}{N_a}+\frac{1}{N_d}\right)\right]^{1/2}, \tag{3}$$

where $V_0 = (k_b T_c/e)\ln\left(N_a N_d/n_i^2\right)$ is the built-in voltage of the p-n junction at equilibrium, ε_s is the permittivity of GaSb, n_i the intrinsic carrier concentration, N_a and N_d are the density of acceptors and donnors in the p and n regions, respectively.

Optics EXPRESS

The boundary conditions required to solve the minority carrier transport equations assume that there is no excess carrier at the edge of the depletion region. Solving Eq. (2) gives the short circuit current J_{sc} under illumination. To retrieve the dark current $J_{\text{dark}}(V)$, Eq. (2) is solved under dark condition ($G = 0$) for several applied voltages (V) on the PV device. The boundary conditions are modified to account for the applied voltage, such as the excess density of the minority carriers at the edges of the depletion region is

$$\Delta n,\ p = n_0,\ p_0 \exp\left(\frac{eV}{k_b T_c}\right). \tag{4}$$

Here, n_0 and p_0 are the electron and hole density at equilibrium, e the charge of electron, k_b the boltzmann constant and T_c the operating temperature of the PV cell.

The current density-voltage characteristics is then calculated using the superposition principle.

$$J = J_{sc} - J_{\text{dark}}(V) \tag{5}$$

The maximum electrical power output Q_{elec} at the optimal applied voltage and the efficiency $\eta = \frac{Q_{\text{elec}}}{Q_{\text{in}}}$, can eventually be extracted. Here, Q_{in} is the net radiative power emitted by the radiator, and also the input power required to maintain the radiator at constant operating temperature T_{rad}, calculated by means of fluctuational electrodynamics. The heat source inside the PV cell Q_{heat} is calculated as

$$Q_{\text{heat}} = Q_{\text{abs}} - Q_{\text{elec}}. \tag{6}$$

It is worth mentioning that external luminescence is omitted in Eq. (2) since it is usually extremely small for most current photovoltaic cells [35].

By solving a thermal balance equation between the heat source inside the cell and the cooling powers of the different mechanisms described in the next section, the operating temperature of the cell can be calculated. An iterative procedure is applied using updated temperature-dependent properties of the cell provided by [28] (i.e. the optical properties of GaSb, the intrinsic carrier concentrations in the p and n regions, the mobilities and diffusion coefficients of the electrons and holes, and the built-in voltage of the p-n junction) until convergence of the temperature. The outputs of the simulations are the system efficiency, maximum power-output and cell operating temperature.

3. Thermal behavior of the GaSb thermophotovoltaic cell

The system under consideration is depicted in Fig. 1(a). A 1D multilayer W-HfO_2 spectrally selective radiator (similar to [18]) at 1500 K radiates thermal energy toward a GaSb p-n junction, grown on a GaSb substrate. The presence of the substrate leads to parasitic sub-bangap absorption, but in this work it is assumed that a substrate is used to grow high-quality p and n-doped layers. Therefore, for the sake of realism, it is assumed that 100μm of the substrate layer is remaining after etching. As a first choice, temperature of the radiator could be selected such that the wavelength of the maximum of the blackbody spectrum at that temperature corresponds to the bandgap of GaSb at 300 K. However, it was shown that the same type of radiators sometime fails to reach thermal stability around 1500 K [22,25,26]. Therefore, we select at first a temperature of 1500 K for the radiator. The thicknesses of the different layers of the radiator are chosen according to [18], such that spectral selectivity is optimized. At the rear of the junction, a gold layer is used as a contact and a backside reflector to recycle photons not absorbed by the cell, by reflecting them back in the cell and eventually to the radiator. Possibly, at the back of the PV device, a radiative cooler, facing the sky, is used to evacuate heat via thermal radiation. Details about the radiative cooler are given in the next section.

The optical properties required for the calculations in the range [0.5 μm - 30 μm] are measured with ellipsometry for W, HfO_2, and taken from [36] for Au. For GaSb, the same model as in

Optics EXPRESS

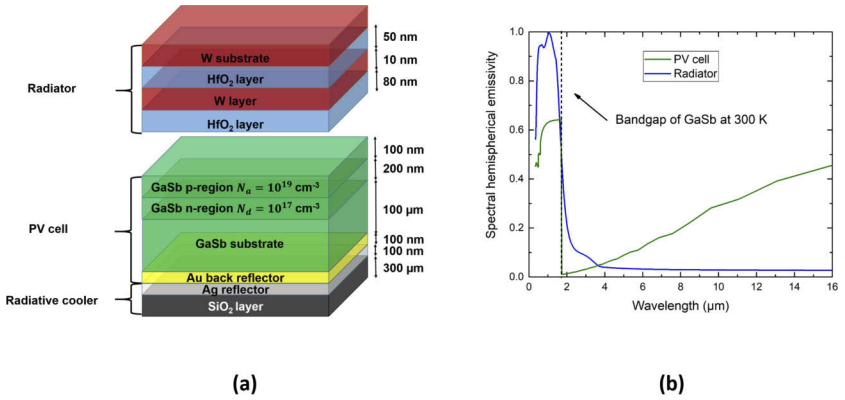

Fig. 1. (a): Schematic representation of the TPV system under study. (b): Spectral hemispherical emissivity of the W-HfO_2 radiator and of the PV device.

[29,34] is used. In Fig. 1(b), the spectral hemispherical emissivity of the selective radiator and of the PV device are plotted. The designed radiator has high emissivity for photons with energy above the bandgap of the PV device, and low emissivity for sub-bangap photons, meaning most of the radiation emitted by the radiator is converted into electron-hole pairs. Using the model presented in the previous section, the loss in efficiency when the cell temperature increases can be quantified.

Indeed Fig. 2(a) shows that efficiency decreases linearly with temperature, then saturates when approaching zero. From the linear part of the curve, the temperature coefficient of the cell, i.e. the loss of efficiency per Kelvin, can be retrieved by linear regression. A value of 0.34 %.K^{-1} is found, which is close to what is reported for GaSb cells [27]. To get more insights into the impact of temperature on the performances of the PV cell, J-V and P-V characteristics are plotted for different temperatures in Fig. 2(b). It is observed that the short-circuit current increases with temperature, due to the narrowing of the bandgap which allows collecting more photons, and also due to a larger absorptivity of GaSb [28]. However, this increase is compensated by a large drop in open-circuit voltage, which eventually leads to a smaller maximum power output.

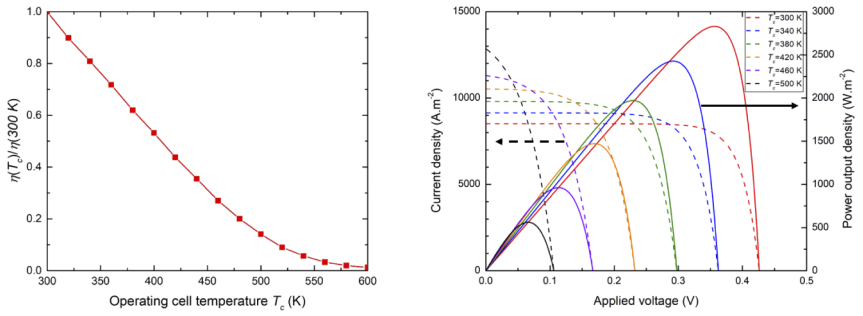

Fig. 2. (a): Loss in efficiency due to thermal losses $\eta(T_c)/\eta(300\text{K})$ as a function of the temperature of the PV device. On the linear part, a temperature coefficient of 0.34 %.K^{-1} is calculated. (b): J-V and P-V characteristics of the PV cell for different operating cell temperatures T_c. The arrows indicate to which y-axis the curves correspond.

Optics EXPRESS

4. Thermal management of the TPV system with conductive-convective and radiative cooling

Conductive-convective heat transfer is considered for cooling the PV device, and its power Q_c is calculated as

$$Q_c = h_c \left(T_c - T_\infty\right). \tag{7}$$

h_c is the conductive-convective heat transfer coefficient and a parameter in this study, T_c is the operating cell temperature and T_∞ is the temperature of the cooling fluid (set at 300 K).

The PV device can also evacuate heat via thermal radiation. For efficient cooling, the device should exchange energy with a body at much lower temperature. In this frame, it is possible to exploit the transparency regions of earth atmosphere in the infrared. In these spectral windows, the device can exchange thermal radiation with the cold outer space, leading to efficient cooling. However, solar radiation has to be reflected by the system in order to avoid heat sources. Surfaces with low emissivity in the solar spectrum and high emissivity in the infrared are required to get maximum cooling power. This is the principle of the so-called daytime radiative cooling, which can be applied to PV cells [37–39]. For TPV devices, we propose to place the radiative cooler at the rear of the cell, facing the sky. As a structure for radiative cooling, we follow the framework of [39]: a layer of glass SiO_2, transparent in the solar spectrum and emissive in the infrared, is used to emit thermal radiation. A silver layer is used to reflect the solar spectrum. With optical indices measured by ellipsometry for Ag and reflectometry for glass SiO_2 [40], the spectral hemispherical emissivity of the radiative cooler is displayed in Fig. 3(a). It is observed that it has low absorption in the spectral range of solar irradiation, and large emission in the infrared, and thus leading to good radiative cooling properties. Normalized solar irradiation [41], blackbody at 300 K and atmosphere transmittance [42] spectra are also plotted for insights. It is worth noticing that the emissivity of the radiative cooler is not selective in the transparency windows of earth atmosphere but rather broadband in the infrared. However, since the radiative cooler is always operating at a temperature larger than the ambient, the net radiative transfer between the radiative cooler and the atmosphere increases the radiative cooling power. By sing the optical properties of the radiative cooler, the radiative cooling power is calculated as

$$\begin{aligned} Q_{\text{rad}} = \int \cos\left(\theta\right) d\Omega \cos \int_0^\infty I_{\text{BB}}\left(T_c, \lambda\right) \varepsilon\left(\lambda, \theta\right) d\lambda \\ - \int d\Omega \cos\left(\theta\right) \int_0^\infty I_{\text{BB}}\left(T_{\text{ATM}}, \lambda\right) \varepsilon^{\text{ATM}}\left(\lambda, \theta\right) \varepsilon\left(\lambda, \theta\right) d\lambda - \int_0^\infty I_{\text{sun}}\left(\lambda\right) d\lambda. \end{aligned} \tag{8}$$

I_{BB} is the blackbody spectral emittance, θ is the incident angle, ε and ε^{ATM} are the spectral directional emissivities of the radiative cooler and the atmosphere, I_{sun} is the solar irradiation power, and T_{ATM} is the temperature of the atmosphere, set at 300 K in this study. $d\Omega$ is related to the integration over the hemisphere. In Eq. (4), the first term corresponds to the radiative power emitted by the structure, the second to the radiative power emitted by the atmosphere and absorbed by the radiative cooler, and the last one to the absorbed solar power.

Considering conductive-convective and radiative cooling, efficiency of the system and the operating cell temperature are calculated as a function of the heat transfer coefficient. Results are displayed in Fig. 3(b). For values of h_c below 100 $\text{W.m}^{-2}\text{.K}^{-1}$, due to the extremely large cell temperature, the efficiency of the TPV system reaches values close to 0. As expected, because of the large heat flux emitted by the radiator at 1500 K, thermal effect arises as a major issue in TPV. It is also observed that to maintain the cell at ambient temperature, a heat transfer coefficient larger than 1000 $\text{W.m}^{-2}\text{.K}^{-1}$ is required, which is of course far beyond what can be obtained with natural convection. The impact of radiative cooling can be observed by comparing the results for the two cases, with and without radiative cooling. At high values of h_c, radiative cooling has no significant impact on the system efficiency, because the conductive-convective cooling power is much larger than the radiative one [43], if the area of the radiative cooler is not

Optics EXPRESS

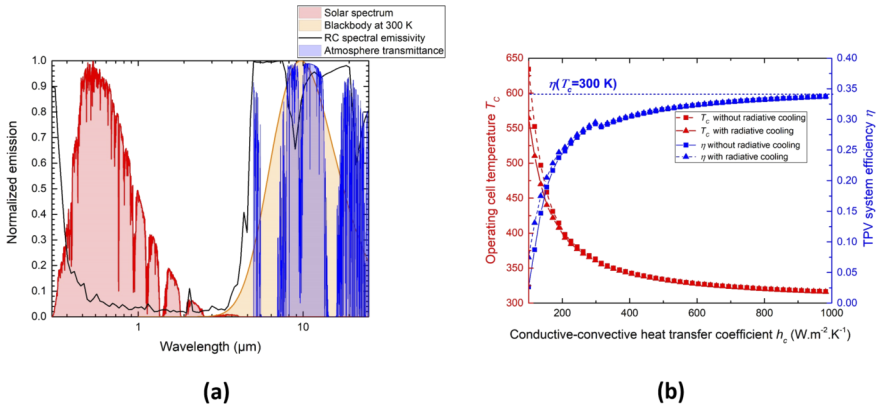

Fig. 3. (a): Normalized solar irradiation spectrum, normalized blackbody emission spectrum at 300 K, spectral emissivity of the radiative cooler and transmittance of earth atmosphere in the infrared. (b): Efficiency and operating temperature of the PV cell as a function of the conductive-convective heat transfer coefficient. The cases with and without radiative cooling are depicted.

much larger than that of the PV cell, like in [39]. When values of h_c get lower, radiative cooling contributes to decreasing the cell temperature and therefore increasing the system efficiency. However, this occurs in the regime where efficiency has already dropped significantly from its value at 300 K. Therefore, radiative cooling is not a suitable solution for decreasing efficiently the cell temperature in this configuration.

As a summary for this section, to reach acceptable efficiencies, the conductive-convective heat transfer coefficient has to be of the order of 100 W.m^{-2}.K^{-1}. For example, to mitigate the thermal losses and reach 90 % of the efficiency at 300 K, h_c has to reach around 600 W.m^{-2}.K^{-1}, which is far beyond what can be obtained with passive conductive-convective cooling systems. Furthermore, because the thermal sources are so important, passive radiative cooling using only the area of the PV cell is not efficient to keep the cell at acceptable temperatures. A solution to tackle this problem is to decrease the thermal emission of the radiator to mitigate heat sources inside the PV cell. This is investigated in the next section.

5. Mitigating the heat source in the PV cell by decreasing the radiator thermal emission

5.1. Decreasing the spectral emissivity of the radiator

To tackle the problem of the increase in temperature of the PV cell, one solution can be to decrease the radiator emissive power. The first way to do so is to reduce the emissivity of the thermal radiator. In the following, we consider a selective radiator at 1500 K with no emission for photon energies below the bandgap of the PV cell, and a constant emissivity for photon energies above. In Fig. 4(a), efficiency is depicted as a function of h_c for different emissivities of the thermal radiator. It is observed that decreasing thermal emission mitigates the drop in efficiency for low values of h_c. This is due to the fact that the heat source in the PV cell follows the radiator emissive power drop, thus leading to a smaller cell operating temperature. As for power output (Fig. 4(b)), when h_c is large, decreasing emission results in a drop of energy yield by the PV device, since less photons are absorbed. However, when h_c decreases, a regime appears where a radiator with low emission produces a larger power output than a radiator with large emission, due to the mitigation of the thermal losses.

Optics EXPRESS

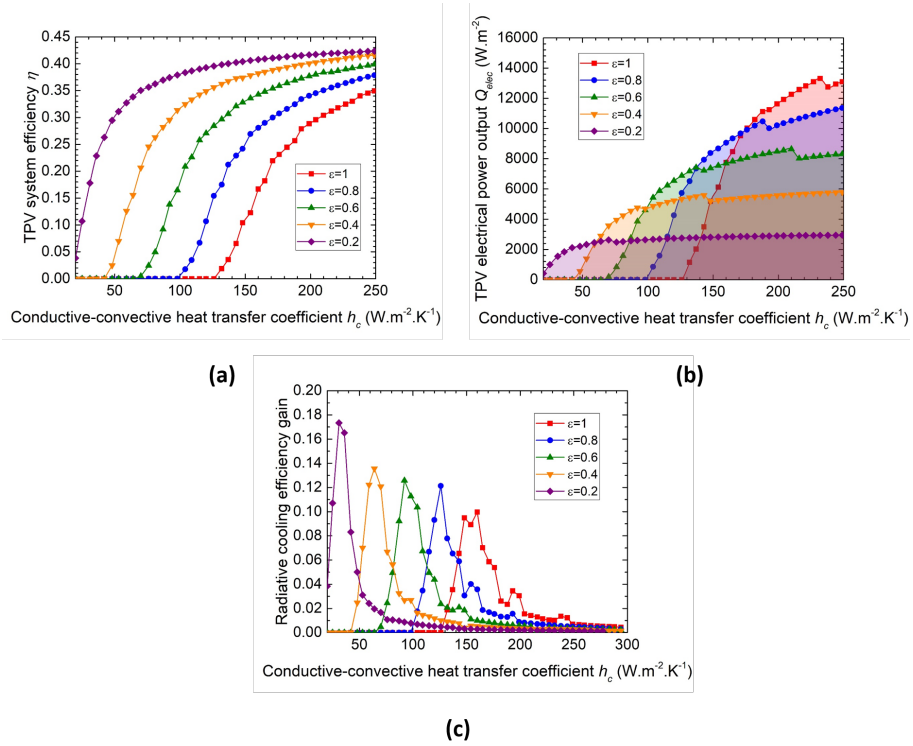

Fig. 4. Performances of the TPV system for a fictitious selective radiator at 1500 K with different emissivities for photon energies above the bandgap as a function of the heat transfer coefficient. (a): Efficiency. (b): Maximum power output. (c): Efficiency gain with radiative cooling as a function of the conductive-convective heat transfer coefficient.

In Fig. 4(c), the gain in efficiency thanks to radiative cooling, i.e. the difference between the efficiency with and without radiative cooling, is depicted as a function of the heat transfer coefficient for different emissivities of the radiator. It is observed that the gain in efficiency reaches a maximum for a given value of h_c. When emission of the radiator decreases, thermal effects become less important at low h_c, and the peak in radiative cooling efficiency gain tends to increase and shifts toward low values of h_c. As a result, decreasing emission of the TPV radiator allows radiative cooling to be more effective on the TPV system performances, and for values of conductive-convective heat transfer coefficient corresponding to passive natural convection. In summary, decreasing emission is beneficial to the efficiency of the TPV system when the heat transfer coefficient is low. It allows radiative cooling the be efficient and to mitigate thermal losses, resulting in a gain in efficiency, and possibly leading to a gain in energy yield by the PV cell despite the decrease of the radiation power incident on the PV device. However, this solution requires a new design of a thermally stable spectrally selective radiator.

5.2. Decreasing the radiator temperature

Another solution to decrease heat sources is to decrease the radiator temperature. However, doing so leads to a shift of the blackbody spectrum toward low photon energies. This means that a smaller part of the blackbody spectrum is located in the spectral range where photons have sufficient energy to produce electron-hole pairs, leading to smaller radiative efficiencies. However, as thermal radiation emission scales with the fourth power of temperature, reducing

Optics EXPRESS

temperature of the radiator can greatly decrease thermal losses, leading to an increase of the efficiency. In Fig. 5(a), the efficiency of the TPV system is plotted as a function of the radiator temperature for several conductive-convective heat transfer coefficients. When the cell is slightly cooled (h_c = 50 W.m^{-2}.K^{-1}), decreasing the radiator temperature leads to an increase of the efficiency due to mitigation of thermal losses. When h_c = 300 W.m^{-2}.K^{-1}, thermal losses are already mitigated by the cooling system and the efficiency decreases due to the blackbody spectrum shift. For h_c = 200 W.m^{-2}.K^{-1}, there is a trade-off between the two phenomena, leading to a local maximum for a given radiator temperature T_{rad}. In summary, decreasing the radiator temperature can have a positive impact on the efficiency if the cooling power is not sufficient. The fact that high temperature is not a mandatory condition for reaching the highest efficiencies in TPV systems can mitigate the constraint of thermal stability. Moreover, it is worth mentioning that in our study, the charge transport problem was solved in 1D without accounting for lateral resistance losses. At high illumination levels, these losses can be large because they are proportional to the square of the electrical current [44]. Therefore, it would mean that decreasing the thermal radiation emission of the radiator would be even more beneficial. Another advantage of decreasing the radiator temperature is that it reduces the amount of input power Q_{in} required to maintain the radiator at a constant operating temperature. This depicted in Fig. 5(b), where the input power is plotted as a function of the radiator temperature. Between 1500 and 1300 K, Q_{in} is decreased by a factor 2, while the electrical power output Q_{elec} gets larger in some cases. In practice, it would be easier to maintain the radiator at a constant operating temperature, and therefore the TPV system would cover a larger range of applications.

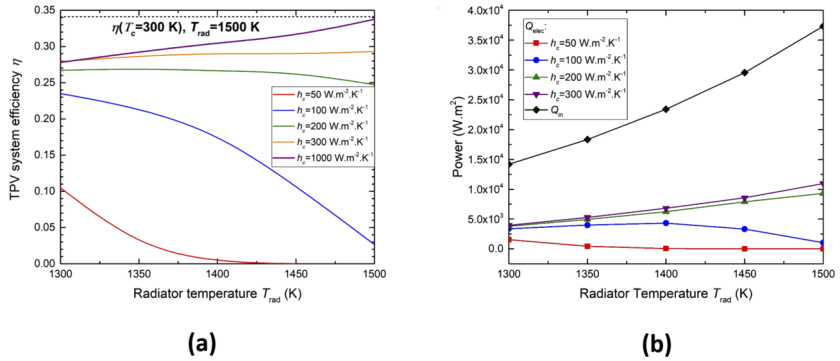

Fig. 5. (a): Efficiency of the TPV system as a fonction of radiator temperature T_{rad} for different values of h_c. (b): Input power Q_{in} (black curve) and electrical power of the PV cell Q_{elec} (colored curves) as a function of the radiator temperature T_{rad}.

6. Conclusions

We have performed simulations of a TPV system composed of a selective radiator at high temperature and a GaSb PV cell. Radiative transfer from the emitter to the PV cell, transport of electrical charges inside the GaSb p-on-n junction and the operating temperature of the PV device have been accounted for. We have shown that thermal effects inside the PV cell arise as a major issue, leading to extremely low performances of the system if the conductive-convective heat transfer coefficient applied to the device is not sufficiently large. To reach the optimal efficiency, conductive-convective heat transfer coefficients corresponding to active cooling must be considered. Because active cooling systems consume energy, it would decrease the efficiency of the overall system. Passive radiative cooling cannot significantly improve the efficiency if the heat sources inside the PV cell are too large, which is the case for a W-HfO_2 radiator at 1500 K. Decreasing the radiator emission is a suitable solution to mitigate heat sources inside the PV

Optics EXPRESS

device: it allows radiative cooling to be effective, and increase the performances of the PV cell by mitigating thermal effects. Eventually, decreasing the radiator temperature can be a solution. It is worth mentioning that it would also simplify the problem of thermal stability of the radiator, since metallo-dielectric structures have been reported to degrade at temperature around 1500 K [25,26]. Furthermore, in a real system, maintaining a radiator with low emission at its operating temperature would require a less important thermal power source, which would make the TPV system operative for a wider range of applications. Eventually, by assessing that even a TPV device with a designed optimal radiator can have low efficiency, we have shown that the design of a TPV system should be performed by considering the optical properties of both the radiator and the PV cell, the electrical and thermal behaviors of the PV device. This work is therefore a guideline for the design of realistic full TPV systems with high efficiency.

Funding

Agence Nationale de la Recherche (ANR-17-CE06-0002-01).

Disclosures

The authors declare no conflicts of interest

References

1. T. Bauer, *Thermophotovoltaics, Basic Principles and Critical Aspects of System Design* (Springer, 2011).
2. A. Lenert, D. M. Bierman, Y. Nam, W. R. Chan, I. Celanovic, M. Soljacic, and E. N. Wang, "A nanophotonic solar thermophotovoltaic device," Nat. Nanotechnol. **9**(2), 126–130 (2014).
3. M. Shimizu, A. Kohiyama, and H. Yugami, "High-efficiency solar-thermophotovoltaic system equipped with a monolithic planar selective absorber/emitter," J. Photonics Energy **5**(1), 053099 (2015).
4. C. Ungaro, S. K. Gray, and M. C. Gupta, "Solar thermophotovoltaic system using nanostructures," Opt. Express **23**(19), A1149–A1156 (2015).
5. D. M. Bierman, A. Lenert, W. R. Chan, B. Bhatia, I. Celanovic, M. Soljacic, and E. N. Wang, "Enhanced photovoltaic energy conversion using thermally based spectral shaping," Nat. Energy **1**(6), 16068 (2016).
6. A. Datas and A. Martí, "Thermophotovoltaic energy in space applications: Review and future potential," Sol. Energy Mater. Sol. Cells **161**, 285–296 (2017).
7. Z. Omair, G. Scranton, L. M. Pazos-Outón, T. P. Xiao, M. A. Steiner, V. Ganapati, P. F. Peterson, J. Holzrichter, H. Atwater, and E. Yablonovitch, "Ultraefficient thermophotovoltaic power conversion by band-edge spectral filtering," Proc. Natl. Acad. Sci. U. S. A. **116**(31), 15356–15361 (2019).
8. J. G. Fleming, S. Y. Lin, I. E. Kady, and K. M. Ho, "All-metallic three-dimensional photonic crystals with a largeinfrared bandgap," Nature **417**(6884), 52–55 (2002).
9. A. Narayanaswamy and G. Chen, "Thermal emission control with one-dimensional metallodielectric photonic crystals," Phys. Rev. B **70**(12), 125101 (2004).
10. I. Celanovic, D. Perreault, and J. Kassakian, "Resonant-cavity enhanced thermal emission," Phys. Rev. B **72**(7), 075127 (2005).
11. D. L. C. Chan, M. Soljačić, and J. D. Joannopoulos, "Thermal emission and design in 2d-periodic metallic photonic crystal slabs," Opt. Express **14**(19), 8785–8796 (2006).
12. P. Nagpal, S. E. Han, A. Stein, and D. J. Norris, "Efficient low-temperature thermophotovoltaic emitters from metallic photonic crystals," Nano Lett. **8**(10), 3238–3243 (2008). PMID: 18781817.
13. N. P. Sergeant, O. Pincon, M. Agrawal, and P. Peumans, "Design of wide-angle solar-selective absorbers using aperiodic metal-dielectric stacks," Opt. Express **17**(25), 22800–22812 (2009).
14. C. Arnold, F. Marquier, M. Garin, F. Pardo, S. Collin, N. Bardou, J.-L. Pelouard, and J.-J. Greffet, "Coherent thermal infrared emission by two-dimensional silicon carbide gratings," Phys. Rev. B **86**(3), 035316 (2012).
15. E. Nefzaoui, J. Drevillon, and K. Joulain, "Selective emitters design and optimization for thermophotovoltaic applications," J. Appl. Phys. **111**(8), 084316 (2012).
16. V. Rinnerbauer, Y. X. Yeng, W. R. Chan, J. J. Senkevich, J. D. Joannopoulos, M. Soljačić, and I. Celanovic, "High-temperature stability and selective thermal emission of polycrystalline tantalum photonic crystals," Opt. Express **21**(9), 11482–11491 (2013).
17. E. Blandre, P.-O. Chapuis, and R. Vaillon, "Spectral and total temperature-dependent emissivities of few-layer structures on a metallic substrate," Opt. Express **24**(2), A374–A387 (2016).
18. E. Blandre, M. Shimizu, A. Kohiyama, H. Yugami, P.-O. Chapuis, and R. Vaillon, "Spectrally shaping high-temperature radiators for thermophotovoltaics using Mo-HfO_2 trilayer-on-substrate structures," Opt. Express **26**(4), 4346–4357 (2018).

Optics EXPRESS

19. T. Burger, D. Fan, K. Lee, S. R. Forrest, and A. Lenert, "Thin-film architectures with high spectral selectivity for thermophotovoltaic cells," ACS Photonics **5**(7), 2748–2754 (2018).
20. P. N. Dyachenko, J. J. do Rosário, E. W. Leib, A. Y. Petrov, M. Störmer, H. Weller, T. Vossmeyer, G. A. Schneider, and M. Eich, "Tungsten band edge absorber/emitter based on a monolayer of ceramic microspheres," Opt. Express **23**(19), A1236–A1244 (2015).
21. P. N. Dyanchenko, S. Molesky, A. Y. Petrov, M. Stormer, T. Krekeler, S. Lang, M. Ritter, Z. Jacob, and M. Eich, "Controlling thermal emission with refractory epsilon-near-zero metamaterials via topological transitions," Nat. Commun. **7**(1), 11809 (2016).
22. M. Chirumamilla, A. S. Roberts, F. Ding, D. Wang, P. K. Kristensen, S. I. Bozhevolnyi, and K. Pedersen, "Multilayer tungsten-alumina-based broadband light absorbers for high-temperature applications," Opt. Mater. Express **6**(8), 2704–2714 (2016).
23. Z. Zhou, E. Sakr, Y. Sun, and P. Bermel, "Solar thermophotovoltaics: reshaping the solar spectrum," Nanophotonics **5**(1), 1–21 (2016).
24. J. H. Kim, S. M. Jung, and M. W. Shin, "High-temperature degradation of one-dimensional metallodielectric (W/SiO_2) photonic crystal as selective thermal emitter for thermophotovoltaic system," Opt. Mater. **72**, 45–51 (2017).
25. M. Shimizu, A. Kohiyama, and H. Yugami, "Evaluation of thermal stability in spectrally selective few-layer metallo-dielectric structures for solar thermophotovoltaics," J. Quant. Spectrosc. Radiat. Transfer **212**, 45–49 (2018).
26. M. Chirumamilla, G. V. Krishnamurthy, K. Knopp, T. Krekeler, M. Graf, D. Jalas, M. Ritter, M. Störmer, A. Y. Petrov, and M. Eich, "Metamaterial emitter for thermophotovoltaics stable up to 1400 C," Sci. Rep. **9**(1), 7241 (2019).
27. O. Dupré, R. Vaillon, and M. A. Green, *Thermal behaviour of photovoltaic devices. Physics and engineering*. (Springer, 2017).
28. M. Francoeur, R. Vaillon, and M. P. Menguc, "Thermal impacts on the performance of nanoscale-gap thermophotovoltaic power generators," IEEE Trans. Energy Convers. **26**(2), 686–698 (2011).
29. M. P. Bernardi, O. Dupré, E. Blandre, P. O. Chapuis, R. Vaillon, and M. Francoeur, "Impacts of propagating, frustrated and surface modes on radiative, electrical and thermal losses in nanoscale-gap thermophotovoltaic powergenerators," Sci. Rep. **5**(1), 11626 (2015).
30. J. DeSutter, M. P. Bernardi, and M. Francoeur, "Determination of thermal emission spectra maximizing thermophotovoltaic performance using a genetic algorithm," Energy Convers. Manage. **108**, 429–438 (2016).
31. S. M. Rytov and I. U. A. Kravtsov, *Principles of Statistical Radiophysics: Elements of random fields*. (Springer-Verlag, 1989).
32. D. Polder and M. Van Hove, "Theory of radiative heat transfer between closely spaced bodies," Phys. Rev. B **4**(10), 3303–3314 (1971).
33. M. Francoeur, M. P. Menguc, and R. Vaillon, "Solution of near-field thermal radiation in one-dimensional layered media using dyadic green's functions and the scattering matrix method," J. Quant. Spectrosc. Radiat. Transfer **110**(18), 2002–2018 (2009).
34. E. Blandre, P.-O. Chapuis, and R. Vaillon, "High-injection effects in near-field thermophotovoltaic devices," Sci. Rep. **7**(1), 15860 (2017).
35. M. A. Green, "Radiative efficiency of state-of-the-art photovoltaic cells," Prog. Photovolt: Res. Appl. **20**(4), 472–476 (2012).
36. E. Palik, *Handbook of Optical Constants of Solids 1rst edition* (Academic Press, 1987).
37. L. Zhu, A. Raman, K. X. Wang, M. A. Anoma, and S. Fan, "Radiative cooling of solar cells," Optica **1**(1), 32–38 (2014).
38. B. Zhao, M. Hu, X. Ao, and G. Pei, "Performance analysis of enhanced radiative cooling of solar cells based on a commercial silicon photovoltaic module," Sol. Energy **176**, 248–255 (2018).
39. Z. Zhou, Z. Wang, and P. Bermel, "Radiative cooling for low-bandgap photovoltaics under concentrated sunlight," Opt. Express **27**(8), A404–A418 (2019).
40. D. D. S. Meneses, M. Malki, and P. Echegut, "Optical and structural properties of calcium silicate glasses," J. Non-Cryst. Solids **352**(50-51), 5301–5308 (2006).
41. Solar Spectral Irradiance: Air Mass 1.5. http://rredc.nrel.gov/solar/spectra/am1.5/ (accessed Oct. 13 2016).
42. IR Transmission Spectra: Gemini Observatory. https://www.gemini.edu/sciops/telescopes-and-sites/observing-conditionconstraints/ir-transmission-spectra (accessed Oct. 13 2016).
43. R. Vaillon, O. Dupré, R. B. Cal, and M. Calaf, "Pathways for mitigating thermal losses in solar photovoltaics," Sci. Rep. **8**(1), 13163 (2018).
44. R. Vaillon, J.-P. Pérez, C. Lucchesi, D. Cakiroglu, P.-O. Chapuis, T. Taliercio, and E. Tournié, "Micron-sized liquid nitrogen-cooled indium antimonide photovoltaic cell for near-field thermophotovoltaics," Opt. Express **27**(4), A11–A24 (2019).